NEOPLASMA accepted, ahead of print manuscript
Cite article as https://doi.org/10.4149/neo_2026_250916N395

Running title: ABCD3 as a therapeutic target in colorectal cancer

Prognostic model based on mitochondrial genes highlights ABCD3 as a potential therapeutic target in colorectal cancer

Shuyu Chen[1,2,#], Youyue Li[1,#], Wenbo Ding[1,2,#], Yujuan Yin[1], Xiaoqi Xin[1,2], Xueyang Wei[1,2], Siqi Bao[1], Bei Pan[3,*], Huiling Sun[1,3,*], Mu Xu[2,3,*]

[1]General Clinical Research Center, Nanjing First Hospital, Nanjing Medical University, Nanjing, China; [2]School of Basic Medicine and Clinical Pharmacy, Nanjing First Hospital, China Pharmaceutical University, Nanjing, China; [3]Department of Laboratory Medicine, Nanjing First Hospital, Nanjing Medical University, Nanjing, China.

Received September 16, 2025 / Accepted April 1, 2026

*Correspondence: panbei9656@163.com; sunhuiling1988@yeah.net; xumu@njmu.edu.cn

[#]Contributed equally to this work.

Studies have shown that abnormal mitochondrial function is closely associated with the development and progression of colorectal cancer (CRC); however, prognostic models based on mitochondria-related genes are still lacking. We systematically analyzed the expression of mitochondrial-related genes in CRC patients and constructed and validated a mitochondrial gene risk prognostic model using various bioinformatics methods across the TCGA and GEO databases. We also investigated the effects of tumor microenvironment, immune cell infiltration, tumor mutation load, and drug sensitivity on patient prognosis. In addition, we overexpressed the ABCD3 gene using CRISPR-dCas9 technology and further explored the role of ABCD3 in cell proliferation and apoptosis by protein blotting and flow cytometry.

The mitochondrial gene risk model was effective in predicting the prognosis of CRC patients, which showed that the high-risk group was significantly different from the low-risk group in terms of immune cell infiltration. Further analyses revealed a strong association between risk scores and clinicopathological features, immune infiltration, and drug sensitivity.

We constructed a prognostic prediction model based on mitochondria-related genes and found that ABCD3 provides a novel biomarker for the individualized treatment of CRC.

Key words: prognostic model; ABCD3; mitochondrial genes; biomarker; colorectal cancer (CRC)

CRC is one of the leading causes of morbidity and mortality worldwide, posing a significant threat to human health. Studies indicate that the overall survival rate for CRC remains low, with both

incidence and mortality rates continuing to rise globally [1]. According to the International Agency for Research on Cancer, by 2040, new cases are projected to reach 3.2 million, and deaths are expected to increase to 1.6 million. These projections highlight the urgent need for improved research, prevention, and treatment strategies for CRC [2]. The development of CRC is closely linked to the tumor microenvironment, including inflammatory responses and genetic factors, as well as lifestyle-related risk factors such as population aging, dietary habits, obesity, lack of physical activity, and smoking. Nearly half of CRC patients die from metastatic disease [3]. Over the past decade, the life expectancy of CRC patients has improved, with median overall survival (OS) ranging from 32 to 40 months. These improvements are largely due to advancements in systemic therapies, local treatment strategies, and novel therapeutic approaches validated through clinical trials [4]. However, CRC remains a prevalent malignancy globally and is the third leading cause of cancer-related deaths worldwide [1]. Early detection and screening can reduce CRC mortality, and the removal of precancerous lesions can decrease its incidence [1]. Therefore, preventive measures through screening technologies are crucial for reducing the incidence of CRC.

There is increasing evidence that mitochondria play a critical regulatory role in cell growth, apoptosis, and metabolism during tumor progression [5]. Mitochondria are involved in essential bioenergetic processes, such as ATP production, reactive oxygen species (ROS) generation, apoptosis regulation, and calcium homeostasis [6]. Mitochondrial dysfunction can contribute to chemotherapy resistance [7]. Furthermore, in the context of chronic injury, mitochondrial dysfunction is believed to act as an initiating factor in CRC tumorigenesis. In diagnosed CRC, altered mitochondrial metabolism promotes tumor growth. Therapeutic strategies targeting mitochondria may provide complementary approaches to existing treatments and could be tailored to specific patient subtypes according to biomarkers, including genetic mutations, metabolic profiles, or indicators of mitochondrial stress [8].

Given the complex relationship between mitochondrial damage and CRC progression, we developed a novel mitochondrial-related risk model (Study diagram) using the ABCD3, TRAP1, DNAJC28, PLSCR3, and RTL10 genes to systematically investigate their impact on CRC prognosis. This mitochondrial-based risk model underscores the potential of these genes to serve as reliable prognostic biomarkers. Through a comprehensive analysis of mitochondrial-associated features, we revealed the intricate interconnections between the risk subgroups and clinical characteristics,

cellular composition, tumor immune infiltration, and drug sensitivity. Additionally, we explored the relationship between the risk gene ABCD3 and CRC prognosis, identifying ABCD3 as a potential therapeutic target for CRC. In summary, our mitochondrial-related risk model not only functions as a robust prognostic tool but also provides novel insights into potential therapeutic strategies for precision management of CRC.

Materials and methods

Collection. Data were downloaded from the TCGA database (https://portal.gdc.cancer.gov/) and included 701 cases of CRC RNA-seq samples. Thirteen cases were excluded due to incomplete clinical information or a survival period shorter than 30 days. Thus, a total of 688 samples were analyzed, comprising 637 tumor samples and 51 healthy samples. Validation data were obtained from the Gene Expression Omnibus (GEO) database, specifically GSE14333, GSE17536, GSE17537, GSE38832, and GSE39582 (https://www.ncbi.nlm.nih.gov/geo/). The list of mitochondria-related genes was obtained from the MitoCarta 3.0 database (https://www.broadinstitute.org/mitocarta/mitocarta30-inventory-mammalian-mitochondrial-proteins-and-pathways) [9] and gene set enrichment analysis (https://www.gsea-msigdb.org/gsea/msigdb/index.jsp) [10, 11].

Identification of differentially expressed genes (DEGs). We utilized the "limma" package in R (version 4.4.0) to identify differentially expressed genes (DEGs) between normal and tumor samples, as well as between high-risk and low-risk groups. The criteria for defining DEGs were set as $|\mathrm{Log}_2 \text{ (fold change)}| > 2$ and an adjusted p-value < 0.01. A volcano plot was generated using the "Gdc Volcano Plot" package in R to visualize the DEGs, while a Venn diagram was employed to illustrate the common DEGs shared between the identified DEGs and mitochondrial-related genes.

Construction and validation of mitochondria-related risk scoring labels. Mitochondria-related genes were selected via univariate Cox regression, LASSO regression, and multivariate Cox regression analyses to establish a novel prognostic gene signature. Samples were stratified into low-risk and high-risk groups based on the risk score (using the median cutoff value). The optimal cutoff values and Kaplan-Meier (K-M) survival curves were analyzed using the R packages "survival" and "survminer" to assess the prognostic markers' survival outcomes. The predictive efficacy was evaluated using Receiver Operating Characteristic (ROC) curves, risk plots, and the

concordance index (C-index). Detailed information on the prognostic genes was obtained from The Human Protein Atlas (HPA, https://www.proteinatlas.org/) and the National Center for Biotechnology Information (NCBI, https://www.ncbi.nlm.nih.gov/).

Evaluation of clinical characteristics in the risk model. We included mitochondrial-associated risk features and clinical parameters (age, sex, pathological status, and TNM staging) as covariates. Differential analysis was conducted to compare clinical parameters between high-risk and low-risk groups. The predictive accuracy of the risk features was assessed using the "survivalROC" package.

Correlation analysis of immune cell infiltration. We used the R package CIBERSORT to calculate the abundance of 22 types of tumor-infiltrating immune cells (TIICs) in CRC samples, in order to assess immune cell infiltration. Spearman correlation analysis was performed to explore associations between selected genes, risk scores, and immune cell infiltration.

Construction and validation of the nomogram. A nomogram incorporating age, pathological stage, pathological T/N/M stages, and risk scores was constructed using the R package "rms". Calibration curves were employed to assess the concordance between predicted probabilities and actual events. The C-index was utilized to measure the predictive accuracy of the model. The analysis of calibration curves examined the consistency between predicted events and observed occurrences. Furthermore, comparative analysis based on the C-index was conducted to evaluate the predictive performance of age, pathological stage, pathological T stage, pathological N stage, pathological M stage, risk scores, and the nomogram score.

Gene ontology (GO) and Kyoto encyclopedia of genes and genomes (KEGG) analyses. In this study, the R packages 'clusterProfiler', 'org.Hs.eg.db', 'richplot', and 'ggplot2' (R version: 4.4.0) were employed to analyze the functional enrichment of mitochondrial-related differentially expressed genes (DEGs) between the high-risk and low-risk groups. Functional candidates were further selected using an adjusted P-value threshold of < 0.05.

Gene set enrichment analysis (GSEA). Biological characteristics of differentially expressed genes (DEGs) were explored using the R package "clusterProfiler," which includes Gene Set Enrichment Analysis (GSEA). Gene sets were considered statistically significant when $p < 0.001$ and FDR $q < 0.001$. The results were visually represented using the R package "ggplot2."

Mutation analysis. We compared mutations in mitochondria-related genes between the high-risk and low-risk subgroups using the Mutation Annotation Format (MAF) data from the TCGA

database by using an R package called 'maftools'.

Analysis of drug sensitivity in patients with different risk scores. This study utilized the Genomics of Drug Sensitivity in Cancer (GDSC) dataset to conduct a drug sensitivity analysis, exploring the predictive capability of risk scores for responses to immunotherapy and 138 chemotherapeutic/targeted therapy agents. The analysis aimed to determine the differences in drug responses among various risk groups.

Cell lines and cultivation. HEK-293T (RRID: CVCL_0063) and Human CRC cell lines HT-29 (RRID: HTB-38) were obtained from ATCC. The cells were cultured in McCoy's 5A medium (KGM4892S-500, KeyGen Biotech, Jiangsu, China) and DMEM (KGM12800S-500, KeyGen Biotech, Jiangsu, China), respectively. Both media were supplemented with 10% fetal bovine serum (FBS) and 10% penicillin-streptomycin. The cells were incubated at 37 °C in a humidified atmosphere with 5% CO_2 .

ABCD3 overexpressed via CRISPR-dCas9 system. The sgRNA sequence targeting ABCD3 using CRISPR-dCas9 (Supplementary Table S1) was predicted through the GPP portal (https://portals.broadinstitute.org/gppx/crispick/public) and synthesized by Shanghai Shenggong Biotechnology Co, Ltd. This sequence was then inserted into the corresponding CRISPR-dCas9 vector, lentiSAMv2, to form a complete plasmid. Subsequently, a gene knockout lentivirus was generated using a lentiviral packaging system composed of HEK-293T cells, the target plasmid, packaging plasmids, and envelope plasmids. HT-29 cells were seeded in six-well plates and transfected with the lentivirus. After 7 days of puromycin selection, stable ABCD3-dCas9-sg cells were established. Control cells were transfected with the empty vector, lentiSAMv2. The gene knockout efficiency was validated by Western blotting and qPCR.

Western blotting (WB). ABCD3 dCas9 sg cells and negative control HT-29 cells were harvested and washed thoroughly with phosphate-buffered saline (PBS). Protein extraction was then carried out using lysis buffer. The primary antibodies used in this study were ABCD3 (#A18177, ABclonal), CDK4 (#11026-1-AP, Proteintech), Cyclin D1 (#60186-1-Ig, Proteintech), BAX (#50599-2-Ig, Proteintech), and GAPDH (#60004-1-Ig, Proteintech), with GAPDH serving as the loading control. Protein expression was analyzed using a chemiluminescence imaging system (Model 5200, Tanon, Shanghai, China) and AllDoc_x software.

RNA extraction and RT-qPCR analysis. Total RNA was extracted from tissue samples using the

RNA-easy reagent (#R711-01, Vazyme, Jiangsu, China). The concentration, purity, and quantity of the RNA were assessed using a multifunctional plate reader. Complementary DNA (cDNA) was synthesized by reverse transcription (RT) using the ABclonal RT Premix (#RK20429, ABclonal, Hubei, China). Real-time quantitative PCR (RT-qPCR) was performed using the QuantStudio™ 5 Real-Time PCR System (#A28575, Thermo Fisher Scientific, Massachusetts, USA). RT-qPCR assays were conducted in triplicate biological samples. Ct values were obtained using the default threshold settings. GAPDH was used as an endogenous control. Gene primer sequences are provided in Supplementary Table S2.

Clone formation. To assess the proliferative capacity of HT29 cells overexpressing ABCD3, the cells were first digested, and the resulting cell suspension was centrifuged. The HT29 cell line overexpressing ABCD3 was then resuspended and plated into 6-well plates at a density of 6×10^3 cells/well. After a two-week incubation period, the cell colonies were fixed with 4% paraformaldehyde for 15 min and subsequently stained with 10% crystal violet for 15 min. Excess dye was removed by washing with PBS, and the colonies were allowed to dry. The number of colonies formed was then observed and counted.

Cell cycle analysis. HT29 cells overexpressing ABCD3 were collected by centrifugation after enzymatic digestion and washed twice with PBS. The cells were then slowly resuspended in pre-cooled 70% ethanol, and the cell pellet was fixed at 4 °C overnight. The following day, the cells were processed according to the experimental protocol. Subsequently, the cells were stained with a mixture of RNase A and propidium iodide (PI) and incubated at 37 °C for 30 min before being analyzed by flow cytometry.

Apoptosis. HT29 cells overexpressing ABCD3 were collected by centrifugation after enzymatic digestion and washed twice with PBS. This overexpression was further validated using a V-FITC/PI double-staining assay, followed by analysis with a flow cytometer. The experimental data were processed using FlowJo 8.0 software (FlowJo LLC, Franklin Lakes, NJ, USA).

EdU. Cultivate 2×10^6 cells/well in a 24-well plate overnight. The following day, perform EdU labeling using a 2× EdU working solution (20 μM), pre-warmed to 37 °C. Afterward, fix the cells with 4% paraformaldehyde, wash with PBS, and permeabilize using PBS containing 0.3% Triton X-100. Label the cells with a fluorescent probe using the Click Additive Solution, followed by fluorescence detection.

CCK-8. Cell Viability Assay Cell viability was assessed using the Cell Counting Kit-8 (CCK-8) assay (#C0038, Beyotime, China) according to the manufacturer's instructions. Briefly, HT-29 cells transfected with ABCD3-overexpression dCas9 vectors or negative control vectors were seeded into 96-well plates at a density of 2×10^3 cells/well. The cells were cultured for 0, 1, 2, 3, 4 and 5 days. At each time point, 10 μl of CCK-8 reagent was added to each well, and the plates were incubated at 37 °C for 1 h. The absorbance (optical density, OD) was measured using a microplate reader.

Caspase-3/7 activity assay. The activity of Caspase-3/7 was detected using a Caspase-3/7 Activity Assay Kit (#G8090, Promega, USA) following the manufacturer's protocol. Briefly, transfected HT-29 cells were seeded into 96-well plates at a density of 5×10^3 cells/well and cultured for 48 h. Subsequently, 100 μl of Caspase-3/7 reagent was added to each well. After shaking the plate for 30 s and incubating at room temperature for 1 h in the dark, the signal intensity was measured using a microplate reader. Relative Caspase-3/7 activity was normalized to the control group.

Statistical analysis. All statistical analyses were performed using R software. Kaplan-Meier analysis and the log-rank test were employed to evaluate and compare survival rates. A two-tailed p-value of < 0.05 was considered statistically significant.

Results

Identification and functional enrichment analysis of mitochondria-associated DEGs in CRC. A total of 10,929 differentially expressed genes (DEGs) were identified and visualized by comparing the volcano maps of the normal group and the tumor group, and the screening criteria was log2FoldChange > 1 and padj < 0.05 (Figure 1A). Next, mitochondria-associated genes selected from Gene Set Enrichment Analysis (GSEA) and the 10,929 DEGs were co-analyzed in CRC (Figure 1B), resulting in the identification of 190 candidate mitochondria-associated DEGs. Gene Ontology (GO) enrichment analysis was then performed to investigate the critical roles of these mitochondria-associated DEGs in CRC. These DEGs were found to be involved in processes such as small molecule catabolism and the regulation of mitochondrial organization. In terms of cellular components, they are predominantly associated with the mitochondrial matrix and the mitochondrial outer membrane. In terms of molecular function, these DEGs are implicated in small GTPase-mediated signal transduction, DNA-binding transcription factor binding, among others (Supplementary Figure S1A). Furthermore, Kyoto Encyclopedia of Genes and Genomes (KEGG)

pathway analysis demonstrated the involvement of these DEGs in several key pathways, including the MAPK signaling pathway, Ras signaling pathway, chemokine signaling pathway, Hippo signaling pathway, and processes such as the cell cycle and apoptosis (Supplementary Figure S1B).

Construction and validation of mitochondria-related risk signatures. To analyze the expression patterns of mitochondria-associated genes, we performed univariate Cox regression analyses ($P < 0.05$, Figure 1C) on the 190 mitochondria-related differentially expressed genes (DEGs) identified earlier. From this analysis, 13 genes were selected as potential prognostic risk factors for CRC. LASSO regression analysis further refined the selection, reducing the number of candidate genes to 10. Subsequently, multivariate Cox regression analyses (Figures 1D, 1E) narrowed the gene list down to five. Ultimately, five mitochondria-associated DEGs-ABCD3, TRAP1, DNAJC28, PLSCR3, and RTL10-were used to construct a prognostic model for CRC patients (Supplementary Table S3). As shown in Figure 1F, the expression levels of TRAP1, PLSCR3, and RTL10 were higher in tumor samples compared to normal tissues, while the expression of ABCD3 and DNAJC28 was lower. Based on literature evidence, these genes have been confirmed to play critical roles in mitochondrial structure and function: ABCD3 facilitates mitochondrial fatty acid transport and maintains redox homeostasis [12]; TRAP1 regulates mitochondrial protein folding, oxidative phosphorylation, and ROS generation [13]; DNAJC28 preserves mitochondrial protein quality and integrity [14]; PLSCR3 participates in mitochondrial membrane remodeling and apoptosis regulation [15]; RTL10, though less characterized, may influence mitochondrial function and contribute to CRC progression. These functional insights support their inclusion in the prognostic model. Ultimately, the risk score for each CRC patient in the training and validation cohorts was calculated using the following formula:

Risk score=0.022 * ABCD3 - 0.008 * TRAP1 - 0.986 * DNAJC28 + 1.44 * PLSCR3 - 0.037 * RTL10. Patients were categorized into high- and low-risk subgroups based on the median risk score. Kaplan-Meier (K-M) curves demonstrated that patients in the high-risk group had significantly worse overall survival (OS) ($p=0.0009$, Figure 2A). To evaluate the accuracy of the prognostic risk model in predicting OS at 1, 3, and 5 years, receiver operating characteristic (ROC) curves were plotted, yielding area under the curve (AUC) values of 0.687, 0.715, and 0.752, respectively (Figure 2B). The relationships between risk scores, survival time, survival status, and risk ranking, along with heatmaps depicting the expression of the four genes, are presented in Figures 2C and 2E.

Taken together, these results underscore the robustness of our risk model in predicting the prognosis of CRC patients. The robustness of the prognostic risk model was further validated in the GSE14333, GSE17537, GSE38832, GSE39582, and GSE17536 datasets. Consistent with the training cohort, the validation cohort also showed that patients in the high-risk group had poorer outcomes (Figure 2D). Kaplan-Meier curves for the four genes revealed that high expression of PLSCR3 was associated with worse OS (p=0.0009, Figure 1G), while low expression of ABCD3, TRAP1, DNAJC28, and RTL10 was associated with worse OS.

Correlation analysis between prognostic models and clinicopathological characteristics. To comprehensively examine the relationship between the risk model and clinical characteristics, the Wilcoxon rank-sum test was applied to evaluate associations between risk groups and clinical features, including age, gender, tumor stage, and TNM staging (Figure 2F). A significant age difference was observed when comparing the high-risk and low-risk subgroups. In the initial univariate Cox regression analysis, clinicopathological factors such as age, tumor stage, T, M, and N staging, along with the risk score model, were identified as significant predictors of overall survival (OS). To improve prognostic accuracy, these factors were combined to construct a nomogram predicting 1-, 2-, and 3-year OS probabilities (Figure 2G). This integrated approach enhanced the predictive performance of the risk model.

Functional enrichment analysis of DEGs in high-risk and low-risk groups. Functional enrichment analyses were conducted on 466 DEGs between high-risk and low-risk groups. GO enrichment analysis revealed that the biological processes associated with these DEGs were primarily involved in DNA replication (Figure 3A). The cellular component annotations of the DEGs were predominantly enriched in the mitochondrial matrix. In terms of molecular functions, the DEGs were mainly enriched for ubiquitin-dependent protein transaminase activity. KEGG pathway analysis indicated that the enriched pathways were largely related to the cell cycle, cellular autophagy, cellular senescence, apoptosis, protein processing in the endoplasmic reticulum, and ubiquitin-mediated protein degradation (Figure 3B). Additionally, we performed GSEA on the RNA-seq data to identify gene sets associated with high and low CRC risk. Notably, the high-risk group was enriched in pathways related to cellular localization, molecular function, keratin formation, and nucleosome organization, whereas the low-risk group was associated with DNA double-strand break repair, recombination repair, ATP-dependent processes, DNA-dependent

ATPase activity, and ATP hydrolysis activity (Figure 3D).

Mutation patterns in high-risk and low-risk groups. We constructed mutation profiles for both the high-risk and low-risk groups in CRC and analyzed the relationship between risk scores and mutation patterns. As shown in Figure 1C, the top 20 high-frequency mutated genes in both the high-risk and low-risk groups are listed. Among the top five mutated genes, the mutation rates of ADID1A and SYNE1 were reduced in the high-risk group (Figure 3C).

Impact of the risk model on CRC immune response and drug sensitivity. The immune scores between high- and low-risk groups were systematically evaluated using the CIBERSORT algorithm, revealing significant differences (Figure 4A). A notable difference was observed in mast cell resting between the high- and low-risk groups, while no significant changes were found in other immune cell types (Figure 4B). In the high-risk group, multiple positive correlations were observed among LM22 immune cell types, whereas this correlation was reduced in the low-risk group. The extent of TME cell infiltration reflected the immune differences between the two groups (Figure 4C). Using the ssGSEA algorithm to calculate immune cell and immune-related function scores, we found differences in tumor-infiltrating lymphocytes, neutrophils, Th1 cells, and type II interferon responses between the high- and low-risk groups (Figures 4D, 4E). Additionally, when assessing the correlation between risk scores and cancer-targeted drug response (Figure 3E), our study found that the high-risk group exhibited increased sensitivity to 5-FU, oxaliplatin, the mitochondrial inhibitor Dihydrorotenone, and the PI3K/AKT pathway inhibitor Ipatasertib, compared to the low-risk group (Figure 3F). These findings provide insights into potential therapeutic strategies based on risk scores and mitochondrial-related genes.

ABCD3 as a potential therapeutic target for CRC. Among the five genes constituting the risk model, we focused on ABCD3 based on preliminary experiments and existing reports. ABCD3 is known to encode a protein that belongs to the ATP-binding cassette (ABC) transporter superfamily. ABC proteins are involved in the transport of various molecules across both the extracellular and intracellular membranes, playing a role in the input of peroxisomal fatty acids and/or acyl-CoAs into organelles [11]. GO enrichment analysis indicated that ABCD3 is associated with the mitochondrial inner membrane and mitochondrial respiration (Figure 5A). By ranking the TCGA-CRC data based on ABCD3 expression, we incorporated the top 25% high-expression data and the bottom 25% low-expression data for Gene Set Enrichment Analysis (GSEA). Interestingly,

in addition to enrichment in pathways related to cell growth, cell migration, and intercellular component breakdown, differential expression genes were also associated with intercellular signaling (Figure 5B). We further examined whether ABCD3 is associated with the tumor microenvironment through Spearman's correlation analysis. The results showed that ABCD3 was significantly correlated with regulatory T cells (Tregs), M2 macrophages, and CD4+ T cells (Figures 5C, 5D). Moreover, we used maftools to analyze the mutation data of the high-low expression subgroup of ABCD3 gene, and the results showed that ABCD3 was significantly correlated with TP53 and KRAS mutations (Figure 5E).

To experimentally validate the bioinformatics analysis, we generated ABCD3-overexpressing HT-29 cells using CRISPR-dCas9 technology and confirmed the efficiency of overexpression by Western blotting and qPCR (Figures 6A-6C). We next explored the relationship between ABCD3 overexpression and CRC. Compared to the negative control (NC), ABCD3-overexpressing cells showed increased expression of the apoptosis-related protein BAX and decreased expression of cell cycle-related proteins CDK6 and CCND1 (Figure 6B). Flow cytometry further revealed that, compared to the NC, ABCD3-overexpressing cells exhibited a higher apoptosis rate and a significantly increased proportion of cells in the G2/M phase, consistent with our previous screening results (Figures 6F, 6G). In addition, CCK-8 assay results demonstrated that ABCD3 overexpression significantly suppressed the growth and viability of HT-29 cells at different time points (Supplementary Figure S2A). Meanwhile, Caspase-3/7 activity assays showed that ABCD3 overexpression markedly enhanced apoptosis in colorectal cancer cells (Supplementary Figure S2B), further functionally validating the critical role of ABCD3 in inhibiting tumor cell proliferation and promoting apoptosis. Clonogenic assays and EDU experiments also confirmed that ABCD3-overexpressing CRC cells had enhanced proliferative capacity compared to the control group (Figures 6D, 6E). Immunohistochemical staining of CRC tissues and paired non-cancerous tissues confirmed significantly lower ABCD3 expression in tumor tissues (Figure 6H). These findings suggest that ABCD3 is closely related to CRC proliferation and apoptosis, indicating its crucial role in the development and progression of CRC.

Discussion

In recent years, molecular targeted therapies have become the first-line treatment for personalized

and combined therapy in CRC, significantly improving patient survival [16]. Mitochondrial dysfunction is considered a key initiating factor in CRC carcinogenesis [17]. In CRC patients, mitochondrial metabolism contributes to tumor growth, as mitochondria play crucial roles in cell proliferation and apoptosis, making them attractive drug targets [18]. Consequently, targeting mitochondria offers opportunities for both therapy and prognostic assessment [19]. Currently, mitochondria-related genes are being explored as therapeutic targets focusing on metabolic reprogramming, structural abnormalities, and quality control disorders, including glycolysis and oxidative phosphorylation [20]. Increasing evidence shows that mtDNA and related mitochondrial proteins are expected to play a role in early diagnosis and prognosis assessment [21, 22].

In this study, we first performed differential expression analysis using the TCGA-CRC database to identify genes related to mitochondria. The differentially expressed genes (DEGs) were then paired to construct a prognostic model, followed by Cox regression and LASSO regression analyses. The predictive performance of the model was subsequently validated in the training cohort and five independent validation cohorts. Subsequently, we evaluated the relationship between risk scores and clinical pathological features, immune infiltration, and drug sensitivity.

Notably, in our model, ABCD3 is significantly downregulated in CRC, and higher levels of ABCD3 are associated with poorer prognosis in CRC patients. Considering the important role of mitochondria-related genes in immunotherapy and tumor targeted therapy, we focused on mitochondrial gene ABCD3 and carried out a series of experimental and bioinformatics analyses [23, 24]. ABCD3 encodes a protein that is a member of the ATP-binding cassette (ABC) transporter superfamily [25, 26]. The ABC transporter family has been reported to be involved in the transport of anticancer drugs and tumor resistance [27]; for example, ABCG2 confers resistance to topotecan, mitoxantrone, and daunorubicin [28], whereas ABCD1 has been reported as a diagnostic marker for solid pseudopapillary tumors of the pancreas [29].

However, there is a lack of information regarding how the mitochondrial-related gene ABCD3 interacts with CRC and its potential value in predicting clinical outcomes. By investigating the relationship between ABCD3 and CRC, we found that ABCD3 is a key regulator of CRC proliferation and apoptosis, thus addressing a critical knowledge gap. Immune cells play a crucial role in the tumor microenvironment (TME). The success of cancer immunotherapy relies on a comprehensive understanding of the TME and immune evasion mechanisms, where tumors, stroma,

and infiltrating immune cells interact within a complex network [30-32]. Analysis of immune infiltration based on ABCD3 expression revealed that low ABCD3 levels were significantly associated with regulatory T cells (Tregs) and M2 macrophages [33]. Previous studies have reported that high infiltration of Tregs in the TME is linked to poor prognosis in patients with various cancers [34, 35]. These results suggest that low ABCD3 expression is associated with immune-suppressive cells such as Tregs and M2 macrophages, thereby creating an immune-suppressive microenvironment that hinders CD8+ T cell-mediated clearance of tumor cells. In recent decades, advancements in genomic research and the development of precision-targeted therapies have significantly improved the prognosis of CRC patients, including those with advanced stages [36, 37]. Currently, CRC drugs targeting vascular endothelial growth factor, epidermal growth factor receptor, BRAF V600E, and PDL1 are being used in first-line treatments or incorporated into clinical studies for CRC [38]. Accordingly, we assessed IC50 values for common CRC drugs and targeted agents in high- and low-risk groups. The high-risk group exhibited increased sensitivity to first-line chemotherapeutics, including 5-fluorouracil (5-FU) and oxaliplatin, as well as mitochondrial inhibitors such as Dihydrorotenone and EGFR inhibitors (erlotinib). Collectively, these findings indicate that high-risk patients may derive greater benefit from immunotherapies and targeted therapies relative to low-risk patients.

Several mitochondrial-related gene (MRG) signatures for colorectal cancer have been reported in recent years, including models based on differential expression analysis, regression frameworks, and Mendelian randomization–driven multi-omics integration [39]. These studies have provided valuable insights into the mitochondrial landscape of CRC and improved causal gene prioritization at the population level. However, most existing MRG signatures primarily focus on gene selection and prognostic stratification, with limited experimental validation or exploration of downstream biological and immunological consequences. In contrast, our study builds upon these foundations by integrating a prognostic model with functional validation and tumor microenvironment characterization. Specifically, we experimentally confirmed the role of ABCD3 in regulating CRC proliferation and apoptosis, systematically analyzed immune cell infiltration patterns associated with the risk groups, and evaluated therapeutic sensitivity to chemotherapeutic and targeted agents. This multi-dimensional framework links mitochondrial dysregulation not only to patient prognosis but also to immune modulation and treatment response, thereby providing a more comprehensive

and clinically relevant understanding of mitochondrial-driven CRC progression.

Moreover, we acknowledge the limitations of this study. First, although ABCD3 has been validated at both protein and functional levels, the other four genes in the model (TRAP1, DNAJC28, PLSCR3, and RTL10) have not yet been experimentally validated, which will be addressed in future work. Second, while we used CIBERSORT and TIDE algorithms to analyze immune infiltration, more precise approaches such as single-cell RNA sequencing (scRNA-seq) and multiplex immunohistochemistry (mIHC) would allow for a finer characterization of the tumor immune microenvironment. Future studies will incorporate these technologies to validate and expand our findings. Finally, regarding model construction, we applied LASSO regression to avoid overfitting and select robust prognostic genes. We recognize that more advanced machine learning approaches, such as RFE-XGBoost or random survival forests, may further enhance model performance; however, their interpretability and clinical applicability remain limited. Future studies with larger cohorts may incorporate such approaches to optimize predictive performance and robustness. Overall, our study establishes a validated mitochondria-related prognostic model, experimentally confirms ABCD3 function in CRC proliferation and apoptosis, and highlights the potential for mechanistic studies and clinical translation, including exploring liquid biopsy markers or small molecule inhibitors targeting ABCD3 in combination with standard chemotherapy protocols.

Overall, this study establishes a validated mitochondria-related prognostic model, experimentally confirms the role of ABCD3 in CRC proliferation and apoptosis, and highlights its potential for mechanistic studies and clinical translation, including liquid biopsy markers and small molecule inhibitors targeting ABCD3 in combination with standard chemotherapy. Future investigations may explore specific mechanisms, such as how ABCD3 regulates CRC proliferation/apoptosis through mitochondrial metabolism (e.g., fatty acid transport, oxidative phosphorylation), potential synergistic effects with other mitochondrial genes (e.g., ACADM, CPT1A), and the feasibility of clinical translation via liquid biopsy or targeted therapeutics.

Acknowledgements: This work was supported by Nanjing Medical and Health Scientific Research Project (YKK22104) and China Postdoctoral Science Foundation (2023M731745).

Supplementary data are available in the online version of the paper.

434

435

436

References

[1] BRAY F, LAVERSANNE M, SUNG H, FERLAY J, SIEGEL RL et al. Global cancer statistics 2022: GLOBOCAN estimates of incidence and mortality worldwide for 36 cancers in 185 countries. CA Cancer J Clin 2024; 74: 229-263. https://doi.org/10.3322/caac.21834

[2] ENG C, YOSHINO T, RUÍZ-GARCÍA E, MOSTAFA N, CANN CG et al. Colorectal cancer. Lancet 2024; 404: 294-310. https://doi.org/10.1016/S0140-6736(24)00360-X

[3] SIEGEL RL, MILLER KD, JEMAL A. Cancer statistics, 2018. CA Cancer J Clin 2018; 68: 7-30. https://doi.org/10.3322/caac.21442

[4] KANTH P, INADOMI JM. Screening and prevention of colorectal cancer. BMJ 2021; 374: n1855. https://doi.org/10.1136/bmj.n1855

[5] TANPRASERT P, LIMPAKAN YAMADA S, CHATTIPAKORN SC, CHATTIPAKORN N, SHINLAPAWITTAYATORN K. Targeting mitochondria as a therapeutic anti-gastric cancer approach. Apoptosis 2022; 27: 163-183. https://doi.org/10.1007/s10495-022-01709-0

[6] CHANG J, WU H, WU J, LIU M, ZHANG W et al. Constructing a novel mitochondrial-related gene signature for evaluating the tumor immune microenvironment and predicting survival in stomach adenocarcinoma. J Transl Med 2023; 21: 191. https://doi.org/10.1186/s12967-023-04033-6

[7] RODRIGUES T, FERRAZ LS. Therapeutic potential of targeting mitochondrial dynamics in cancer. Biochem Pharmacol 2020; 182: 114282. https://doi.org/10.1016/j.bcp.2020.114282

[8] HAQUE PS, KAPUR N, BARRETT TA, THEISS AL. Mitochondrial function and gastrointestinal diseases. Nat Rev Gastroenterol Hepatol 2024; 21: 537-555. https://doi.org/10.1038/s41575-024-00931-2

[9] RATH S, SHARMA R, GUPTA R, AST T, CHAN C et al. MitoCarta3.0: an updated mitochondrial proteome now with sub-organelle localization and pathway annotations. Nucleic Acids Res 2021; 49: D1541-D1547. https://doi.org/10.1093/nar/gkaa1011

[10] SUBRAMANIAN A, TAMAYO P, MOOTHA VK, MUKHERJEE S, EBERT BL et al. Gene set enrichment analysis: a knowledge-based approach for interpreting genome-wide expression profiles. Proc Natl Acad Sci U S A 2005; 102: 15545-15550. https://doi.org/10.1073/pnas.0506580102

[11] MOOTHA VK, LINDGREN CM, ERIKSSON KF, SUBRAMANIAN A, SIHAG S et al. PGC-1alpha-responsive genes involved in oxidative phosphorylation are coordinately downregulated in human diabetes. Nat Genet 2003; 34: 267-273. https://doi.org/10.1038/ng1180

[12] RANEA-ROBLES P, CHEN H, STAUFFER B, YU C, BHATTACHARYA D et al. The peroxisomal transporter ABCD3 plays a major role in hepatic dicarboxylic fatty acid metabolism and lipid homeostasis. J Inherit Metab Dis 2021; 44: 1419-1433. https://doi.org/10.1002/jimd.12440

[13] ZHAO H, PARK J, WANG Y, CHOU YJ, LI L et al. Cancer suppresses mitochondrial chaperone activity in macrophages to drive immune evasion. Nat Immunol 2025; 26: 2185-2200. https://doi.org/10.1038/s41590-025-02324-2

[14] GAO H, XING F. A novel signature model based on mitochondrial-related genes for predicting survival of colon adenocarcinoma. BMC Med Inform Decis Mak 2022; 22: 277. https://doi.org/10.1186/s12911-022-02020-3

[15] YAN J, CHEN X, CHOKSI S, LIU ZG. TGFB signaling induces mitophagy via PLSCR3-mediated cardiolipin externalization in conjunction with a BNIP3L/NIX-, BNIP3-,

and FUNDC1-dependent mechanism. Autophagy 2025; 21: 1791-1801. https://doi.org/10.1080/15548627.2025.2483441

[16] XIE YH, CHEN YX, FANG JY. Comprehensive review of targeted therapy for colorectal cancer. Signal Transduct Target Ther 2020; 5: 22. https://doi.org/10.1038/s41392-020-0116-z

[17] MIN HY, LEE HY. Molecular targeted therapy for anticancer treatment. Exp Mol Med 2022; 54: 1670-1694. https://doi.org/10.1038/s12276-022-00864-3

[18] ROTH KG, MAMBETSARIEV I, KULKARNI P, SALGIA R. The Mitochondrion as an Emerging Therapeutic Target in Cancer. Trends Mol Med 2020; 26: 119-134. https://doi.org/10.1016/j.molmed.2019.06.009

[19] ZONG WX, RABINOWITZ JD, WHITE E. Mitochondria and Cancer. Mol Cell 2016; 61: 667-676. https://doi.org/10.1016/j.molcel.2016.02.011

[20] CHANG J, WU H, WU J, LIU M, ZHANG W et al. Constructing a novel mitochondrial-related gene signature for evaluating the tumor immune microenvironment and predicting survival in stomach adenocarcinoma. J Transl Med 2023; 21: 191. https://doi.org/10.1186/s12967-023-04033-6

[21] ZHANG L, CUI Y, ZHOU G, ZHANG Z, ZHANG P. Leveraging mitochondrial-programmed cell death dynamics to enhance prognostic accuracy and immunotherapy efficacy in lung adenocarcinoma. J Immunother Cancer 2024; 12: e010008. https://doi.org/10.1136/jitc-2024-010008

[22] CHIANG JL, SHUKLA P, PAGIDAS K, AHMED NS, KARRI S et al. Mitochondria in Ovarian Aging and Reproductive Longevity. Ageing Res Rev 2020; 63: 101168. https://doi.org/10.1016/j.arr.2020.101168

[23] BORCHERDING N, BRESTOFF JR. The power and potential of mitochondria transfer. Nature 2023; 623: 283-291. https://doi.org/10.1038/s41586-023-06537-z

[24] BAI R, CUI J. Mitochondrial immune regulation and anti-tumor immunotherapy strategies targeting mitochondria. Cancer Lett 2023; 564: 216223. https://doi.org/10.1016/j.canlet.2023.216223

[25] TAWBEH A, GONDCAILLE C, TROMPIER D, SAVARY S. Peroxisomal ABC Transporters: An Update. Int J Mol Sci 2021; 22: :6093. https://doi.org/10.3390/ijms22116093

[26] LI Y, CHEN ZP, XU D, WANG L, CHENG MT et al. Structural insights into human ABCD3-mediated peroxisomal acyl-CoA translocation. Cell Discov 2024; 10: 92. https://doi.org/10.1038/s41421-024-00722-8

[27] ZATTONI IF, DELABIO LC, DUTRA JP, KITA DH, SCHEIFFER G et al. Targeting breast cancer resistance protein (BCRP/ABCG2): Functional inhibitors and expression modulators. Eur J Med Chem 2022; 237: 114346. https://doi.org/10.1016/j.ejmech.2022.114346

[28] LI H, ZHANG SL, JIA YH, LI Q, FENG ZW et al. Imidazo[1,2-a]Pyridine Derivatives as Novel Dual-Target Inhibitors of ABCB1 and ABCG2 for Reversing Multidrug Resistance. J Med Chem 2023; 66: 2804-2831. https://doi.org/10.1021/acs.jmedchem.2c01862

[29] LIU YA, LIU Y, TU J, SHI Y, PANG J et al. ABCD1 as a Novel Diagnostic Marker for Solid Pseudopapillary Neoplasm of the Pancreas. Am J Surg Pathol 2024; 48: 511-520. https://doi.org/10.1097/pas.0000000000002205

[30] SHENDE S, RATHORED J, BUDHBAWARE T. Role of metabolic transformation in cancer immunotherapy resistance: molecular mechanisms and therapeutic implications. Discov Oncol 2025; 16: 453. https://doi.org/10.1007/s12672-025-02238-3

[31] PITT JM, MARABELLE A, EGGERMONT A, SORIA JC, KROEMER G et al. Targeting the tumor microenvironment: removing obstruction to anticancer immune responses and immunotherapy. Ann Oncol 2016; 27: 1482-1492. https://doi.org/10.1093/annonc/mdw168
[32] BADER JE, VOSS K, RATHMELL JC. Targeting Metabolism to Improve the Tumor Microenvironment for Cancer Immunotherapy. Mol Cell 2020; 78: 1019-1033. https://doi.org/10.1016/j.molcel.2020.05.034
[33] LI J, ZHANG Y, QU Z, DING R, YIN X. ABCD3 is a prognostic biomarker for glioma and associated with immune infiltration: A study based on oncolysis of gliomas. Front Cell Infect Microbiol 2022; 12: 956801. https://doi.org/10.3389/fcimb.2022.956801
[34] IZZI V, DAVIS MN, NABA A. Pan-Cancer Analysis of the Genomic Alterations and Mutations of the Matrisome. Cancers (Basel) 2020; 12: 2046. https://doi.org/10.3390/cancers12082046
[35] GUO X, ZHANG Y, ZHENG L, ZHENG C, SONG J et al. Global characterization of T cells in non-small-cell lung cancer by single-cell sequencing. Nat Med 2018; 24: 978-985. https://doi.org/10.1038/s41591-018-0045-3
[36] PAREEK CS, SMOCZYNSKI R, TRETYN A. Sequencing technologies and genome sequencing. J Appl Genet 2011; 52: 413-435. https://doi.org/10.1007/s13353-011-0057-x
[37] INOUE A, DEEM AK, KOPETZ S, HEFFERNAN TP, DRAETTA GF, et al. Current and Future Horizons of Patient-Derived Xenograft Models in Colorectal Cancer Translational Research. Cancers (Basel) 2019; 11: 1321. https://doi.org/10.3390/cancers11091321
[38] KAUFMAN NEM, DHINGRA S, JOIS SD, VICENTE M. Molecular Targeting of Epidermal Growth Factor Receptor (EGFR) and Vascular Endothelial Growth Factor Receptor (VEGFR). Molecules 2021; 26: 1076. https://doi.org/10.3390/molecules26041076
[39] ZHU L, HUANG X, ZHANG F, YANG J, XU Z. Mendelian Randomization Analysis of Mitochondria-Related Genes and Screening of Prognostic Genes in Colorectal Cancer. Cancer medicine 2025; 14: e71012. https://doi.org/10.1002/cam4.71012

Figure Legends

Figure 1. Identification of mitochondria-associated differentially expressed genes (DEGs) and construction of a prognostic risk model using the TCGA-CRC Cohort. A) Volcano Plot of 10,929 Differentially Expressed Genes (DEGs): The plot compares the CRC tumor and normal groups. B) Venn Diagram Showing the Overlap of 10,929 DEGs and 2,030 Mitochondrial Genes: This overlap results in the identification of 190 hub genes. C) Univariate Cox Regression Analysis: This analysis revealed that 19 genes are significantly associated with prognosis in CRC patients. D) LASSO Regression Analysis of 13 Overall Survival (OS)-Related Genes: Cross-validation was performed in the LASSO regression model to select optimal tuning parameters. The horizontal axis represents the log(λ) value, while the vertical axis indicates the partial likelihood deviation. The red dots in the figure correspond to the partial likelihood deviation ± standard error for different tuning parameters.

E) Multivariate Cox Regression Analysis: This analysis identified five genes associated with prognosis in CRC patients. F) Gene Expression of Five Prognostically Relevant Genes in TCGA-CRC. G) Kaplan-Meier Curves of the Five Prognostically Relevant Genes in TCGA-CRC: The survival outcomes for high-risk and low-risk groups are presented, showing overall survival (OS) in patients. ***$p < 0.001$

Figure 2. Validation and clinical correlation analyses of prognostic risk models in both the training and validation cohorts. A, D) Kaplan-Meier survival analysis of risk-related features in the TCGA-CRC training set and five independent validation sets. B) ROC curves for overall survival (OS) based on risk-related features in the TCGA-CRC training cohort. C) ROC curves for predicting 1-, 3-, and 5-year OS in the TCGA-CRC training cohort. E) Distribution of risk scores, survival status (red dots represent deceased patients, green dots represent survivors), and expression levels of the five model genes in the TCGA-CRC training cohort. F) Heatmap illustrating the correlation between high and low-risk score groups and clinicopathological features. G) Schematic illustrating the combined effect of risk scores with age, T-stage, N-stage, M-stage, and overall staging. **$p < 0.01$; ***$p < 0.001$

Figure 3. Enrichment analysis results and drug susceptibility prediction analysis of high and low risk subgroups of TCGA-CRC data. A) Gene Ontology (GO) pathway terms significantly enriched in differentially expressed genes across high- and low-risk subgroups. The vertical axis categorizes the enrichment by Biological Process (BP), Cellular Component (CC), and Molecular Function (MF), with the circle size representing the number of enriched genes. B) Kyoto Encyclopedia of Genes and Genomes (KEGG) pathway terms significantly enriched in differentially overexpressed genes across high- and low-risk subgroups. The circle size corresponds to the number of enriched genes. C) Gene Set Enrichment Analysis (GSEA) identifies distinct gene pathways in the high-risk subgroup. D) Mutational waterfall plot depicting the mutational landscape of high- and low-risk subgroups in the prognostic models. E) Risk score predicts the therapeutic efficacy of drugs in high- and low-risk subgroups. F) Drug sensitivity of high- and low-risk subgroups to 5-FU, oxaliplatin, Dihydrorotenone, and Ipatasertib. P-values are indicated as: NS-not significant; *$p < 0.05$; **$p < 0.01$; ***$p < 0.001$.

Figure 4. Differential immune profiles between high- and low-risk subgroups in the TCGA-CRC dataset. Two risk groups were classified based on the median risk score. A-E) Several algorithms, including CIBERSORT analysis and ssGSEA, were employed to assess the five prognostic-related genes and investigate differences in risk scores among various immune cell types. These methods were used to evaluate the correlation between immune-related cells, risk scores, and signature genes. P-values are presented as: NS-not significant; *p < 0.05; **p < 0.01; ***p < 0.001.

Figure 5. Different gene enrichment results and immune characteristics between high and low expression subgroups of ABCD3 in TCGA-CRC dataset. A) CGA-CRC data set ABCD3 expression of high and low subgroups of differentially expressed genes significantly enriched GO pathway entries. B) SEA identified different gene pathways in the high-low expression group. C, D) Seven immune infiltration algorithms (Xcell, TIMER, QUANTISEQ, MCPCOUNTER, EPIC, Cibersort-ABS, and CIBERSORT) were used to evaluate the association between high and low ABCD3 expression subgroups and the tumor microenvironment in the TCGA-CRC cohort. E) maftools was used to detect gene mutation expression in high-low expression subgroups of ABCD3. P-values are presented as: NS-not significant; *p < 0.05; **p < 0.01; ***p < 0.001.

Figure 6. Overexpression of ABCD3 inhibited the growth and proliferation of CRC cells. A) Overexpression of ABCD3 in HT-29 cells using CRISPR-dCas9 technology. B) Western blot verified the overexpression efficiency of ABCD3, and detected the expression levels of CDK4, CCND1 and BAX. C) qPCR was used to verify the ABCD3 overexpression efficiency of dCas9. D, E) Clone formation assays and EDU experiments examined the colony formation and proliferation capacity of ABCD3 overexpressed cells. F, G) Flow cytometry was used to detect the apoptosis and cycle of ABCD3 overexpression cells. H) The expression of ABCD3 in cancer tissues was detected by immunohistochemical staining of colorectal cancer tissues paired with non-cancer tissues.

Fig. 1 [Download full resolution image]

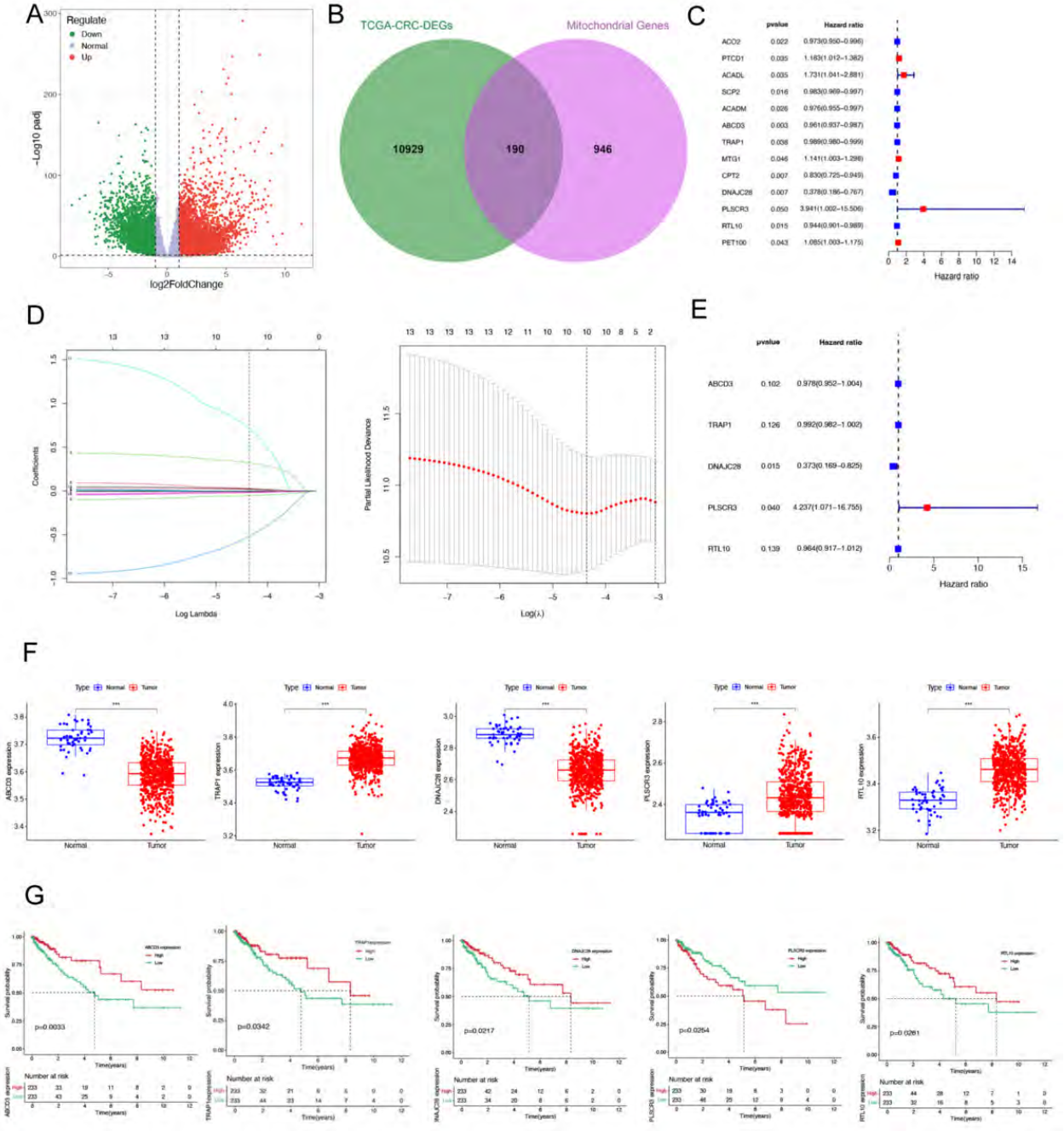

Fig. 2 [Download full resolution image]

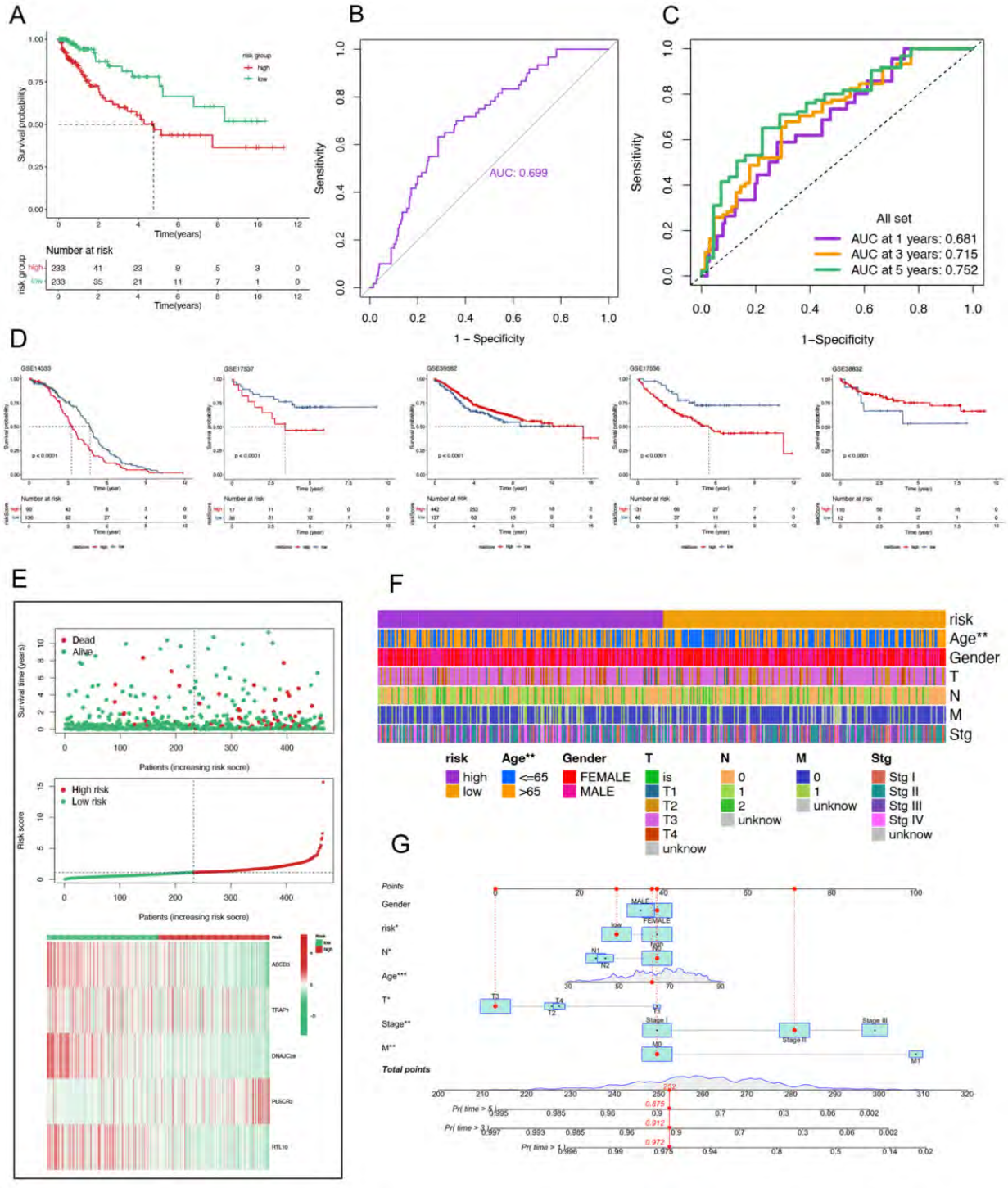

Fig. 3 [Download full resolution image]

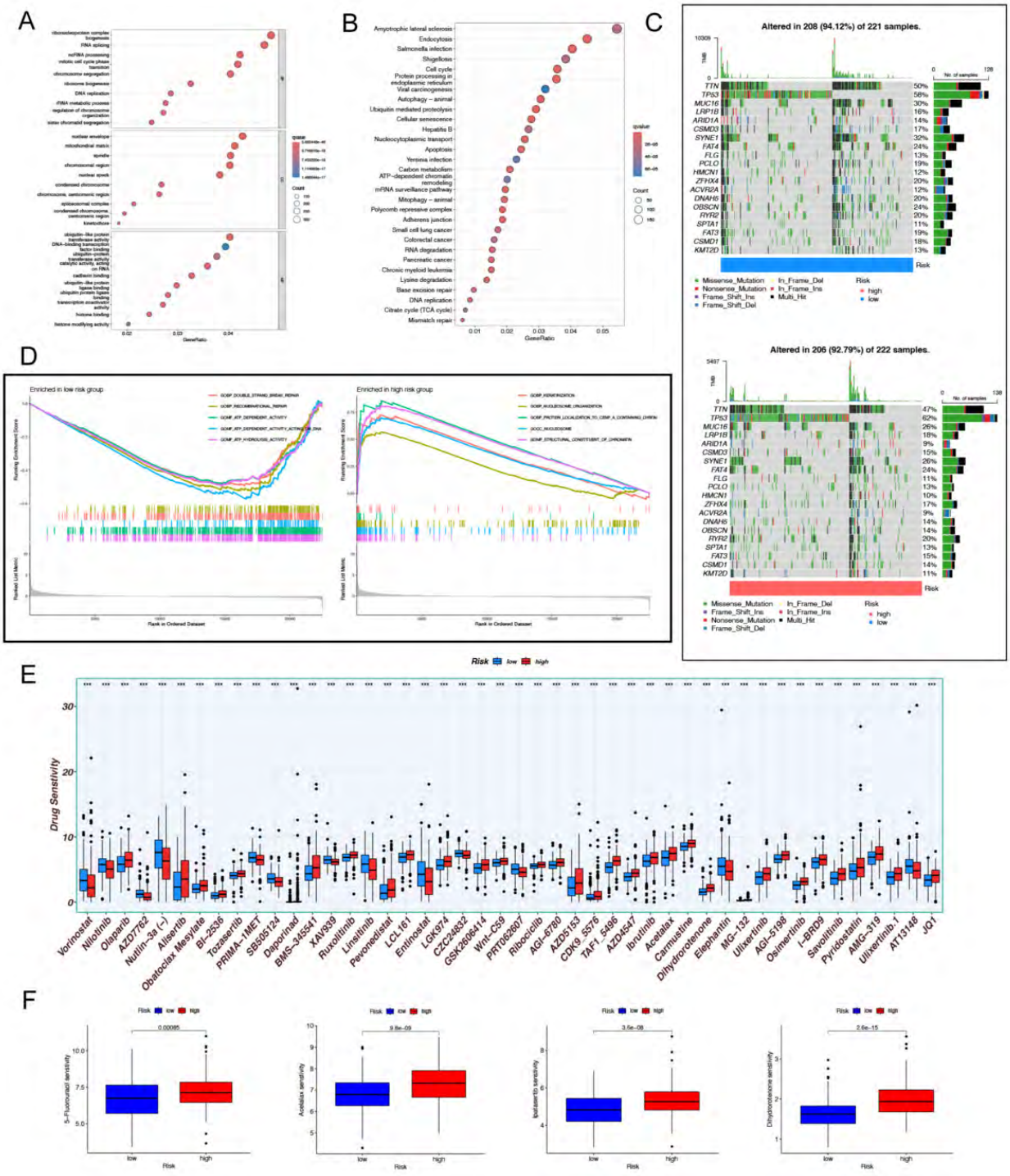

Fig. 4 [Download full resolution image]

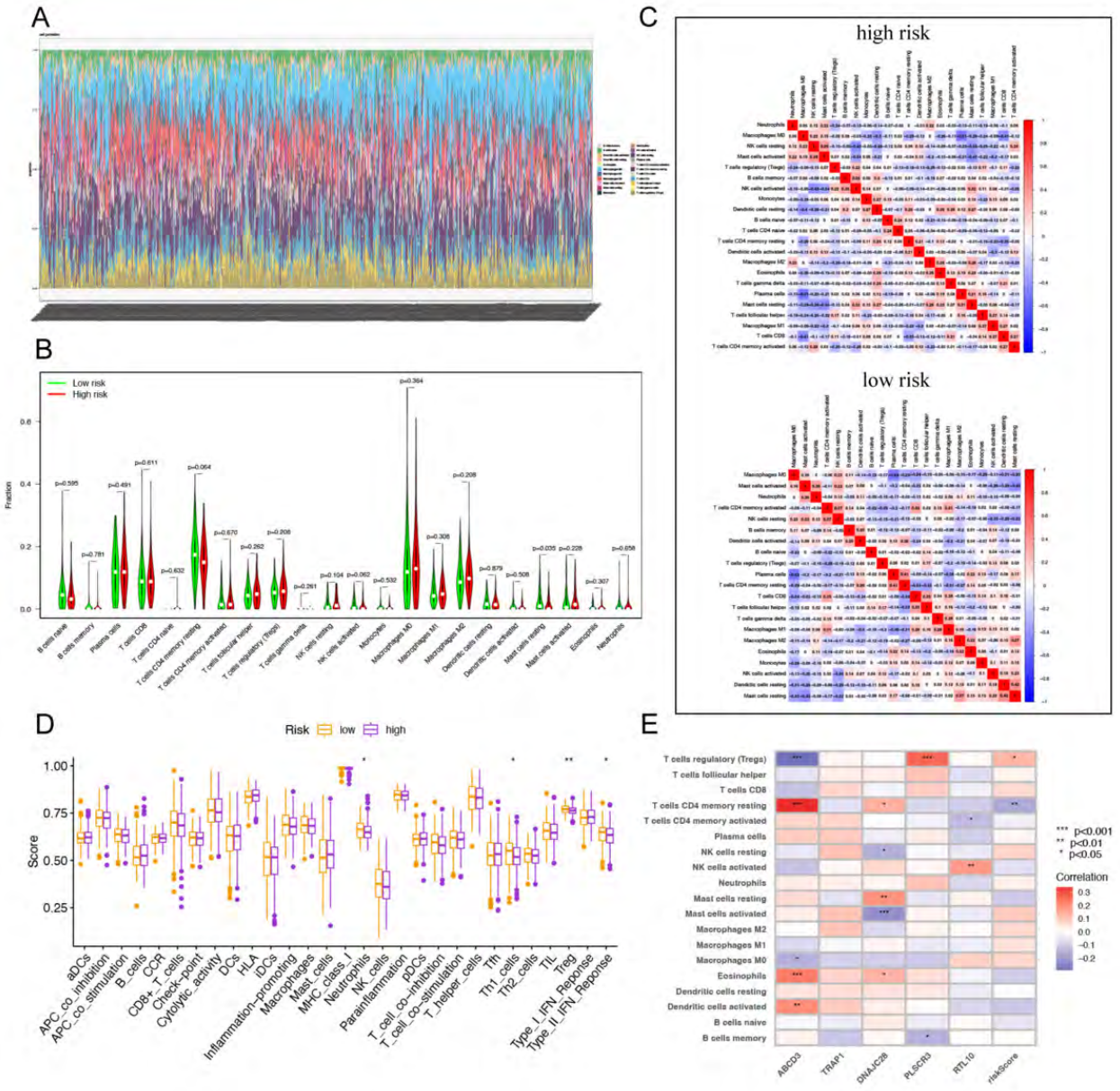

Fig. 5 Download full resolution image

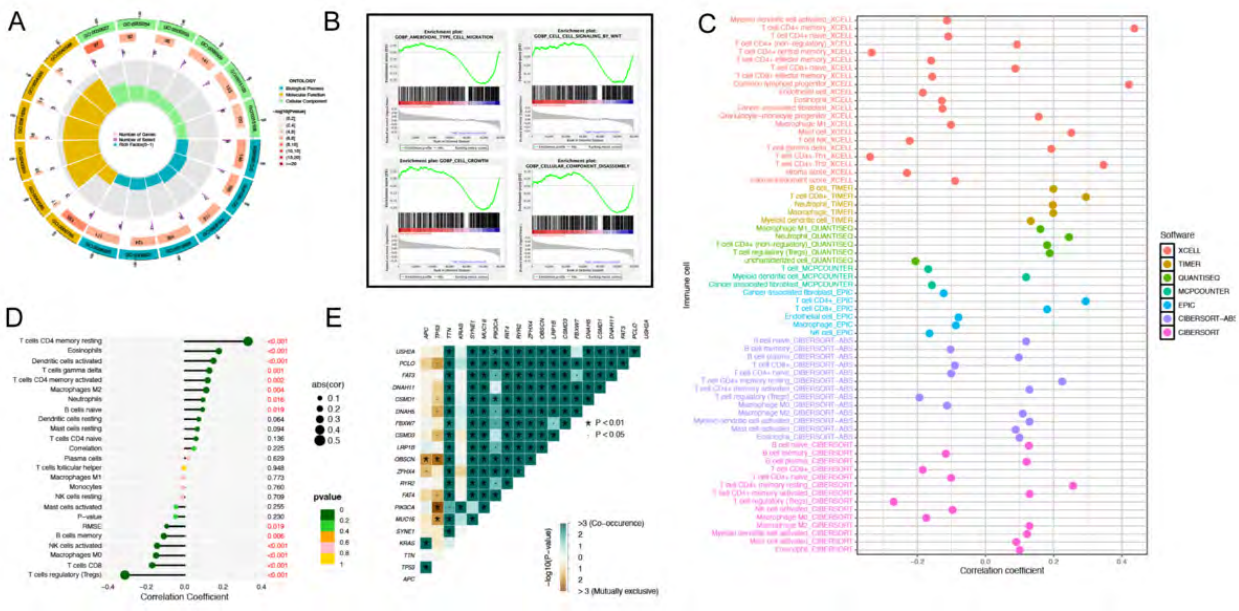

Fig. 6 [Download full resolution image]